CrossMark

TECHNICAL ARTICLE

XRD study of phase transformations in lithiated graphite anodes by Rietveld method

Alexander Missyul,[1,2,a] Ivan Bolshakov,[1] and Roman Shpanchenko[1]
[1]*Battery R&D, Samsung SDI, 130 Samsung-ro, Yeongtong-gu, Suwon 16678, South Korea*
[2]*ALBA Synchrotron Light Source, Carrer de la Llum 2-26, 08290, Cerdanyola del Vallès, Barcelona, Spain*

(Received 14 September 2016; accepted 26 March 2017)

Commercial anodes with different state of charge are investigated by X-ray diffraction technique using Rietveld method for data collected with standard laboratory equipment. It is shown that full profile refinement gives good approximation for quantitative description of the charge/discharge process and may be used for estimation of real state of charge (SoC). Careful analysis of the diffraction profile with Rietveld method allows us to quantitatively distinguish the contribution of different Li_xC_6 phases and estimate the real SoC. © *2017 International Centre for Diffraction Data.*
[doi:10.1017/S0885715617000458]

Key words: lithium-ion batteries, graphite anode, Rietveld analysis, state of charge

I. INTRODUCTION

Lithium-ion batteries nowadays are the main source that powers portable electronic devices, power tools or EV. Improvement of the consumer properties and performance of these batteries demands deep understanding of the phase transformations in electrode materials during their charge and discharge. There are many techniques scrutinizing the structural evolution of electrodes used for both *in situ* and *ex situ* observations. Among them, the diffraction techniques are the most suitable for gathering of the structural information. Synchrotron and neutron sources are mostly used for *in situ* investigations. Because of high beam penetration and sensitivity for light elements, neutron radiation is especially effective for analysis of commercial cylindrical and prismatic batteries (Sharma and Peterson, 2013; Bobrikov *et al.*, 2014; Senyshyn *et al.*, 2015). Synchrotron radiation is used for different types of laboratory made cells and often combined with additional analysis techniques (Bak *et al.*, 2014; Kleiner *et al.*, 2015; Robert *et al.*, 2015). Recently, an *in situ* synchrotron study of rounded 18 650 batteries was also published (He *et al.*, 2015).

Laboratory X-ray diffraction (XRD) remains the most used technique for structural analysis of battery materials because of equipment simplicity and accessibility. Analysis of the XRD data for cathode materials is usually carried out with Rietveld method. Full profile refinement allows us to get reliable structural information, including lattice and atomic parameters and even an estimation of the Li-sites occupancy. Apart from the usual structural data, one may extract additional structural and morphology information hidden in peak profile shapes like size/strain, anisotropic broadening, and perform quantitative phase analysis. Additionally a texture can be analyzed based on intensities of all diffraction peaks. A situation with analysis of laboratory XRD data for graphite anode materials is entirely different. Layered nature of graphite results in a very high-preferred orientation, whereas a big number of structural defects produce different types of strong distortion for diffraction peaks profile (Shi *et al.*, 1993; Iwashita *et al.*, 2004; Wilhelm *et al.*, 2007; Zhou *et al.*, 2014). This high concentration of the structure defects is an intrinsic property of the polycrystalline graphite and cannot be decreased beyond the certain limit. The latter makes Rietveld refinement for graphite materials rather sophisticated and inconvenient.

There are two approaches to overcome those issues. The structural one includes stacking faults modeling. It is more fundamental, but not widely used because of several reasons. Firstly, it demands a special software and only two programs are available nowadays for refinement namely, DIFFaX for stacking fault modeling followed by model refinement using FAULTS or DIFFaX+ programs (Treacy *et al.*, 1991; Dittrich and Wohlfahrt-Mehrens, 2001; Leoni *et al.*, 2004; Johnsen and Norby, 2013; Casas-Cabanas *et al.*, 2016). A special program for full profile refinement of graphite materials was written by Shi *et al.* (1993) and later used by Zhou *et al.* (2014). A usage of these programs for routine analysis is rather inconvenient for many XRD users because of nontrivial model construction and refinement restrictions for multiphasic mixtures. Instead, a comparison of peak positions and intensities is often performed by most authors. In spite of simplicity and representativity, this common approach may lead to some inaccuracy in processes description and especially in their quantification. The inaccuracy appears from an underestimation of contribution made by the Li_xC_6 phases with variable compositions.

The Rietveld method is widely used in academic and industrial laboratories. It does not take into account stacking faults in the materials in details as modeling does: they are hidden in the peak profile shape. Nevertheless, this approach may give reliable general and quantitative structural information sufficient for the most of practical tasks (Li *et al.*, 2009). Additionally, main intercalated Li_xC_6 phases are well distinguished because of their different contribution in full XRD profile.

[a]Author to whom correspondence should be addressed. Electronic mail: amissiul@cells.es

https://doi.org/10.1017/S0885715617000458 Published online by Cambridge University Press

The present work demonstrates that Rietveld analysis for graphite anodes gives satisfying results even with the XRD data obtained by usual powder diffractometer.

II. EXPERIMENTAL

A. Sample

Electrochemical experiments were carried out in half cells at 25 °C. The cells were assembled in the standard coin-type CR2032 cases (diameter 20 mm, height 3.2 mm) using a lithium foil (⌀ 16 mm, thickness 0.7 mm), a porous polyethylene separator, a graphite electrode (⌀ 14 mm), and an electrolyte containing 1.3 M $LiPF_6$ in EC : EMC : DMC (3 : 4 : 3 w/w). Graphite electrodes were obtained from commercial prismatic cells and consisted of 98% graphite, 0.8% carboxymethyl cellulose (CMC) and 1.2% styrene-butadiene rubber (SBR); electrode thickness was 74 μm (including Cu foil thickness 8 μm), density – 1.62 g cm^{-1}. Coin cells were assembled in an Ar-filled glove box.

All cycling tests were performed galvanostatically between 1.5 and 0.01 V (vs. Li/Li^+) at a rate of C/20 (~0.3 mA) using a Bio-Logic VMP3 potentiostat (Bio-Logic, France). Before XRD investigations, the cells were charged to certain SoC (0, 20, 40, and 50%), held 6 h at open-circuit potential and then dismantled in the glove box. Since dQ/dV peaks for $LiC_{30} \rightarrow LiC_{18}$ and $LiC_{18} \rightarrow LiC_{12}$ processes are overlapped (Figure 1), it is impossible to obtain pure LiC_{18}. For simplicity, the charging was stopped at SoC 40% in order to make sure that only LiC_{18} and LiC_{12} exist in the anode. Fully charged LiC_6 is not interesting for the present study and its refinement can be found elsewhere (Guerard and Herold, 1975).

Anode circles taken out from the coin cells were washed with dimethyl carbonate (DMC) to remove electrolyte and covered by kapton film in glove box. Then the XRD patterns were taken in air. Preliminary analysis revealed that during data collection time anodes degrade <2%.

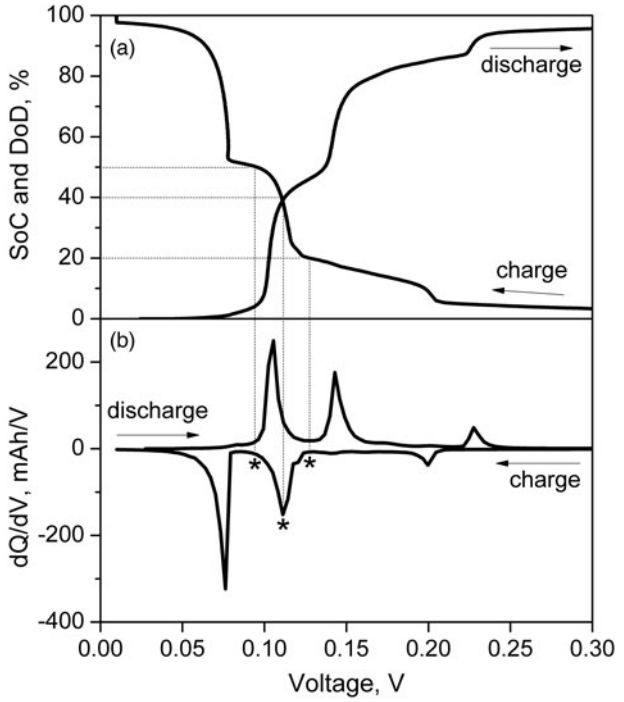


Figure 1. (a) Typical charge/discharge curve of the Li/graphite coin cell (3rd cycle at the rate of C/20) in the voltage range 0.3–0.01 and (b) corresponding differential capacity (dQ/dV) plot. The voltages corresponding to the analyzed samples are marked by the asterisks.

B. Data collection

X-ray powder diffraction data were collected with Philips X-PERT PRO diffractometer (Cu$K\alpha$ radiation, PIXCel SSD, diffracted beam graphite monochromator, 40 kV, and 40 mA) using continuous scan mode (2θ range of 20°–105°, step size 0.013°, scan rate 0.67° min^{-1}, and 300 s $step^{-1}$). The incident slit size (1/2°) was selected taking into account the goniometer radius (240 mm) in such a way to make sure

TABLE I. Crystallographic data for Li_xC_6 compounds.

Phase	Space group	C-layers sequence	a (Å)	c (Å)	Atom	x	y	z	g	Average C–C distance, Å	
										In plane	Interplanar
C	$P6_3/mmc$	(AB)	2.4610(2)	6.7101(1)	C1	0	0	0.25	1	1.421	3.355
					C2	1/3	2/3	0.25	1		
LiC_{30}	$P6_3/mmc$	($ABAACA$)	2.4666(2)	20.8117(4)	C1	0	0	1/4	1	1.424	3.469
					C2	1/3	2/3	1/4	1		
					C3	1/3	2/3	0.4135(2)	1		
					C4	2/3	1/3	0.4135(2)	1		
					Li	0	0	0	1/5[a]		
LiC_{18}	$P6_3mc$	($AABB$)	2.4684(3)	14.0594(7)	C1	0	0	0	1	1.425	3.515
					C2	1/3	2/3	0	1		
					C3	0	0	0.2661(5)	1		
					C4	1/3	2/3	0.2661(5)	1		
					Li	2/3	1/3	0.1331(2)	2/9		
LiC_{12}	$P6/mmm$	(AA)	4.2875(3)	7.0317(2)	C	0.342(2)	0	0.7351(2)	1	1.429	3.516
					Li	0	0	0	1		
LiC_6[b]	$P6/mmm$	(A)(A)	4.316	3.703	C	1/3	0	0	1	1.492	3.703
					Li	0	0	1/2	1		

[a]2/9 for LiC_{27} composition.
[b](Ohzuku *et al.*, 1993).

https://doi.org/10.1017/S0885715617000458 Published online by Cambridge University Press

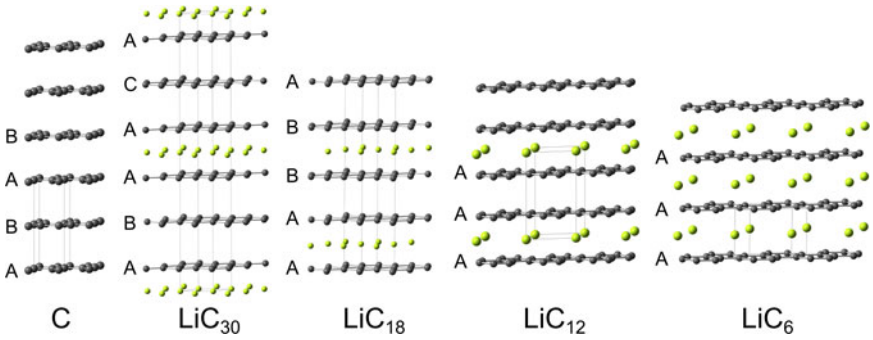


Figure 2. (Color online) Structural transformations in lithiated graphite with ordered Li-layers sequence.

that the size of the irradiated spot remains smaller than the size of the analyzed electrode in the whole measurement range.

C. Data reduction

The obtained diffraction data were converted to the GSAS file format without any additional treatment. Strictly speaking, the high transparency of the graphite layer should lead to the violation of the constant volume assumption and lead to the incorrect determination of the relative peak intensities. However, the contribution of this error is relatively small if there are no low-angle peaks at the diffraction pattern and we did not observe any difference in the refinement results after application of the known corrections to the raw data.

Rietveld refinement was performed using GSAS package (Larson and Von Dreele, 2004) with EXPGUI interface (Toby, 2001). Peak shape and reflection asymmetry owing to axial divergence were described by Pseudo–Voigt function (CW function 3 in GSAS). The March–Dollase function with (001) direction of the preferred orientation was chosen to describe the texture of the anode phases. Occupancies of the Li atoms for LiC_{18} and LiC_{30} phases were fixed, since their refinement resulted in meaningless deviations from the expected values. z coordinates of the C3 and C4 atoms in the LiC_{18} and LiC_{30} phases (Table I) were constrained to be equal in order to keep the corresponding carbon layers flat. Additionally, the fractional coordinate z of the Li atom in the LiC_{18} phase was constrained in such way to position it exactly in the middle of the interlayer space.

Peaks of highly textured copper current collector were fitted using March–Dollase function with three directions of the preferred orientation: (001), (011), (111). Strictly speaking, this should be regarded not as a real orientation in three separate directions but as a series expansion of the real texture. Only the sample shift parameter has physical meaning for the anode phases because of finite thickness of the anode material. This parameter was constrained to be equal for all Li_xC_6 phases. Zero shift for copper phase was refined using both sample shift and transparency corrections.

Peak broadening anisotropy was described by microstrain broadening terms Lij. This description results in a loss of physical information related to stacking faults but it allows one to easily achieve reasonable fitting and to obtain correct structural data and phase composition. Only the Lij terms significantly deviating from zero (usually, L13 and L23) were refined and others were fixed as 0.

Theoretical XRD patterns were calculated in the PowderCell program (Kraus and Nolze, 1996). March–Dollase preferred orientation parameter of 0.7 (that is close to experimental parameters for investigated anodes) was applied.

III. RESULTS AND DISCUSSION

A. XRD for Li–C system

The main structural transformations during intercalation of the Li atoms into graphite and a change of corresponding theoretical XRD patterns are shown in Figures 2 and 3, respectively. This sequence is well known (Ohzuku *et al.*, 1993; Billaud *et al.*, 1996). Position of the first interplanar peak (Figure 3(a)) sequentially decreases with an increase of the Li content and corresponds to average interplanar C–C separation. Three phases in the Li_xC_6 system, namely LiC_6, LiC_{30}, and graphite are well distinguished by their peak positions and intensities. In contrast, the XRD patterns for LiC_{18} and

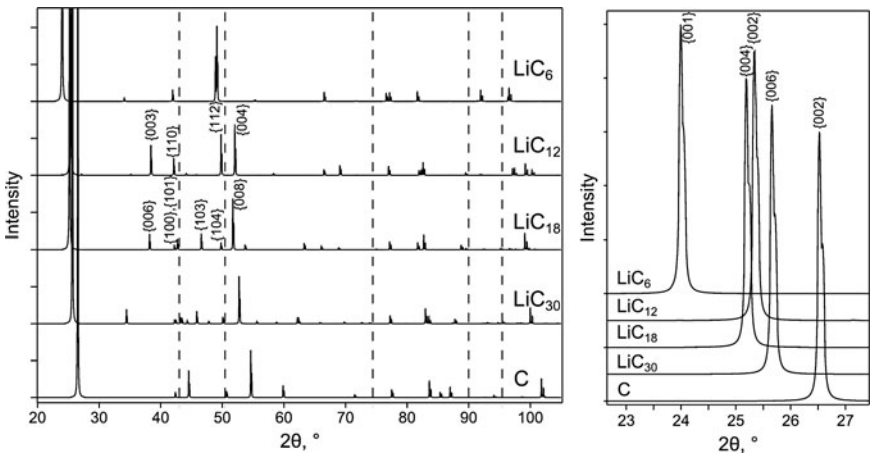


Figure 3. Theoretical XRD patterns for compounds in the Li_xC_6 system. Dash lines indicate position of Cu-peaks from current collector.

https://doi.org/10.1017/S0885715617000458 Published online by Cambridge University Press

LiC_{12} compounds are very similar because of their close lattice parameters ($a_{LiC_{18}} \approx a_{LiC_{12}}/\sqrt{3}$; $c_{LiC_{18}} \approx c_{LiC_{12}} \times 2$) and can be easily mixed up in experimental patterns (Figure 4).

An interpretation of the experimental XRD patterns in some cases may be rather difficult since the real FWHM (full-width at half-maximum) values are usually noticeably bigger than those shown in Figure 3. A strong preferred orientation considerably decreases the number of peaks suitable for phase and structure analysis. Furthermore, a presence of stacking faults contributes in additional changes resulting in distortion of peak shape. Most of the peaks of LiC_{18} & LiC_{12} are strongly overlapped, therefore, careful profile analysis should be used for phase identification and low-intensity peaks become extremely important. Unfortunately, the $\{101\}_{LiC_{18}}$ peak is overlapped with the {111} peak of copper current collector and cannot be used for phase identification. Additionally, the $\{103\}_{LiC_{18}}$ peak is usually strongly broadened because of stacking faults and it becomes almost invisible in the diffraction patterns.

The most prominent difference between these two phases is the strong difference between intensities of the $\{110\}_{LiC_{18}}$ and $\{100\}_{LiC_{12}}$ peaks at ~42.1° and between intensities of the $\{112\}_{LiC_{18}}$ and $\{104\}_{LiC_{12}}$ peaks at ~49.8°. The easiest practical way to distinguish between LiC_{18} & LiC_{12} phases is a structural refinement using full profiles since it takes into account not only peak positions but intensities as well. A correct choice of profile function allows us to perform suitable fitting even when a part of diffraction lines are

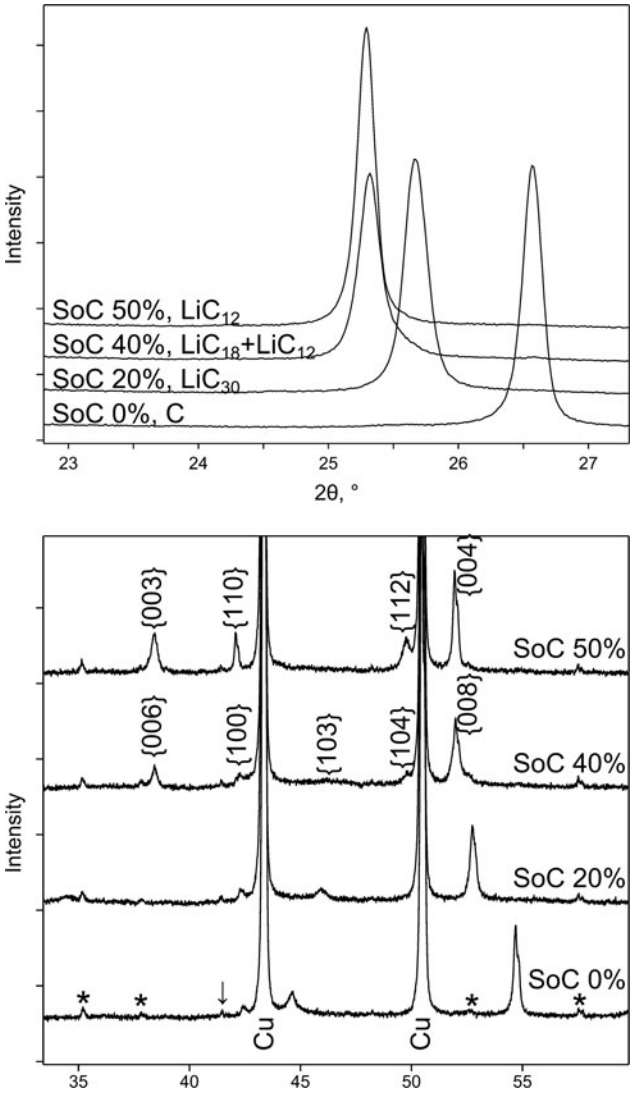


Figure 4. Experimental XRD patterns for anodes with different SoC. Reflections from the Al_2O_3 phase are marked with asterisks.

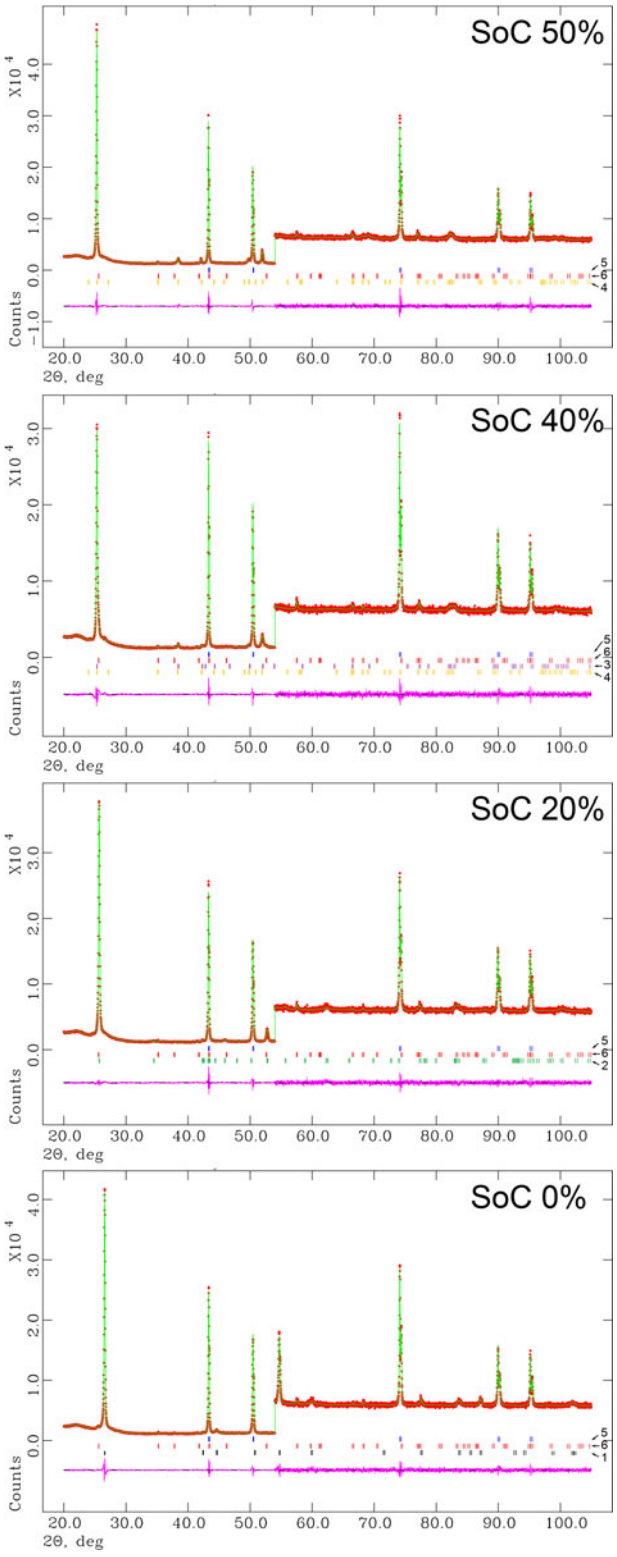


Figure 5. (Color online) Results of Rietveld refinement for anodes with different SoC. Numbers refer to following phases: 1, graphite (black); 2, LiC_{30} (green); 3, LiC_{18} (violet); 4, LiC_{12} (orange); 5, Cu (blue); 6, Al_2O_3 (red).

https://doi.org/10.1017/S0885715617000458 Published online by Cambridge University Press

strongly broadened owing to the presence of stacking faults. Therefore, a contribution of every particular phase in the overall diffraction peak intensity may be determined. Additional and very important practical advantage of structural refinement is the possibility to quantify a weight fraction for every Li_xC_6 phase in the mixture and consequently, estimate a real SoC of anode.

B. Structural characterization

Table I contains crystallographic data for compounds in the Li_xC_6 system. It is worth noting that the structural information for some of Li_xC_6 compounds found in the literature is difficult to use. For example, only layers sequence is given for LiC_{30} (Billaud and Henry, 2002) and a structure of LiC_{18} is reported to depend on the way of its preparation (Billaud *et al.*, 1996). Therefore, we decided to collect the data together for easier usage in the future. Figure 5 shows the result of Rietveld refinement for anodes listed in Table II. One can see from the difference curves the refinement is suitable despite that the XRD data are not of high quality. A use of variable divergent slit for data collection looks more preferable because the X-ray spot fits the electrode area over the whole angle range.

Structural refinement confirmed our above suggestions made by careful phase analysis: it is possible to prove existence of both LiC_{18} and LiC_{12} phases and refine their content. The SoC values were calculated from phase fractions and the SoC values corresponding to each phase. They well correspond to those expected from the charging conditions (Table II).

The main expected differences between the XRD patterns of LiC_{12} and LiC_{18} are intensities of the subcell $\{110\}_{LiC_{12}}/\{100\}_{LiC_{18}}$ and $\{112\}_{LiC_{12}}/\{104\}_{LiC_{18}}$ reflexes and the absence of superstructural $\{103\}_{LiC_{18}}$ peak in the pattern of LiC_{12} (Figure 5). The superstructural $\{103\}_{LiC_{18}}$ peak is strongly broadened owing to the presence of stacking faults and becomes almost invisible in the XRD pattern. The $\{101\}_{LiC_{18}}$ peak is overlapped with the {111} peak of copper and cannot be used for phase identification. Generally, the refinement was carried out mainly with peaks of [00*l*] and [*hk*0] zones. A change of the intensities of the $\{110\}_{LiC_{12}}/\{100\}_{LiC_{18}}$ and $\{112\}_{LiC_{12}}/\{104\}_{LiC_{18}}$ peaks is well visible in Figure 5 for 50 and 40% SoC, respectively. At the same time intensity of the peak at 52° 2θ remains nearly the same with noticeable broadening at 40% SoC in comparison with 50% SoC where only LiC_{12} phase is present. The broadening is because of overlapping of the $\{004\}_{LiC_{12}}$ and $\{008\}_{LiC_{18}}$ peaks.

The values of weight concentrations for every phase give real SoC (Table II). In the proposed case, these values are close to expected ones whereas a refinement 40% SoC pattern as single LiC_{18} leads to a value of SoC 33%.

The size/strain characteristics cannot be extracted or even correctly estimated from the existing data and it was not a goal of the present work. However, it is important to say a few words about texture parameters for Li_xC_6 phases. Texture parameters are different for lithiated phases. For example, in case of the sample used in the current work for refinement of the LiC_{18} structure the March–Dollase coefficients are 0.602 for the LiC_{12} phase and 0.740 for the LiC_{18} phase. This difference means that the naïve determination of the LiC_{18}/LiC_{12} ratio using only the intensities of the strongest peaks would lead to ~2 times smaller value than the real one and corresponding overestimation of SoC. Moreover, the texture parameters vary with a change of state of charge (a detailed study will be published separately). From this point of view a quantification based on intensity ratios for {002} or {004} peaks may result in a noticeable deviation from the real concentration values.

C. Discussion

Detailed guide for the XRD data collection and analysis of graphite materials was published by Iwashita *et al.* (2004). This guide is generally correct for lithiated graphite. Therefore here we pointed out only those features of phase analysis and refinement for Li_xC_6 phases that may be confused at the routine analysis of lithiated anodes.

In this analysis, it was based on a study of lithiated single-crystal graphite carried out by Billaud *et al.* (1996), Billaud and Henry (2002). They obtained and characterized single LiC_{18} and LiC_{30} phases. Because of the LiC_{30} compound was structurally described in (Billaud and Henry, 2002) at the first time one can call it "LiC_{30}" although its real composition is more close to LiC_{27} (Ohzuku *et al.*, 1993). Indeed, it is not important for this work since the difference in these two compositions is negligible and cannot be detected with laboratory XRD data. The LiC_{30} phase is often observed in the strongly discharged or low charged anodes in spite of being rarely mentioned in published literature. Usually it is present in a small amount but including this phase into quantification may noticeably change calculated SoC values for anode. The LiC_{18} phase practically never exists as a single phase at usual cycling conditions. However, its identification in the laboratory XRD patterns may be somewhat confusing because of similarity with the patterns of LiC_{12}.

No doubt, the quality of the XRD data obtained with usual laboratory equipment is noticeably worse in comparison with those taken with synchrotron or neutron radiation. Nevertheless, laboratory *ex situ* measurements remain one of the main tools for analysis of anodes. Our numerous experiments clearly demonstrate that quantitative careful Rietveld refinement always results in reliable and reproducible values. Essential deviations from expected SoC were observed in two cases: (i) for anodes where only surface carbon was lithiated to

TABLE II. Electrochemical characteristics and phase composition for anodes.

Voltage (V)	SoC (%)	Phase composition	Wt (%)	Calculated SoC (%)		
1.205	0	C	100	0		
0.128	20	LiC_{30}		20		
0.111	40	LiC_{18}	80	Two phases[a]	Only LiC_{12}[a]	Only LiC_{18}[a]
		LiC_{12}	17	37	50	33
0.095	50	LiC_{12}	100	50		

[a]Corresponding refining results are shown in Figure 6.

https://doi.org/10.1017/S0885715617000458 Published online by Cambridge University Press

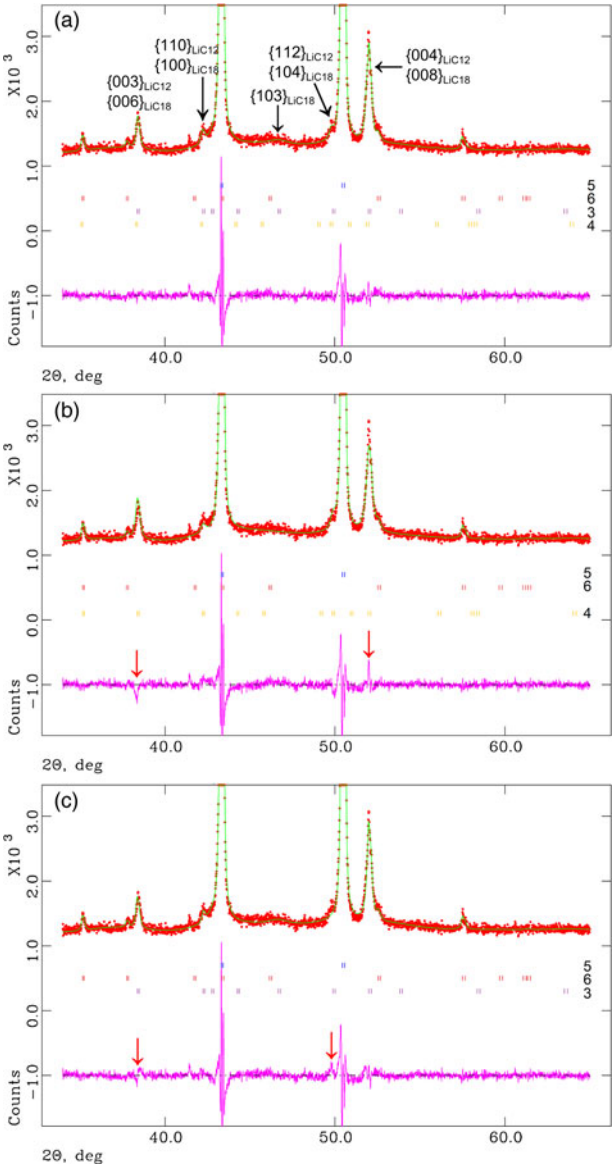


Figure 6. (Color online) Results of Rietveld refinement for anode with 40% SoC: (a) LiC_{12} and LiC_{18} included in the refinement; (b) only LiC_{12} included; (c) only LiC_{18} included. Positions of the most important reflections for analysis are marked by arrows in the difference curves. Colors and phase numbering correspond to Figure 5.

LiC_6 (concluded from color) whereas the bulk contained mixture of LiC_{12} and LiC_{18} phases and (ii) one of Li_xC_6 phases was not accounted in the phase composition. Removing any of them from the refinement leads to visible changes in profile refinement as well as in estimation of the SoC value.

Other phases with smaller Li : C ratio also may be observed at certain conditions (Senyshyn *et al.*, 2013). Nevertheless, in the most practical analysis when high-resolution equipment is not used, consideration of only five phases listed in Table I is sufficient.

IV. CONCLUSIONS

Laboratory XRD equipment was used for quantitative phase analysis of partially lithiated graphite anodes. It was shown that even average quality of XRD data allows us to carry out quantitative analysis and carefully distinguish the contribution of LiC_{12}, LiC_{18}, and LiC_{30} phases in a diffraction pattern. Results of Rietveld refinement demonstrate good agreement between expected and real states of charge for *ex situ* experiments. Detailed refinement procedure is described.

V. SUPPLEMENTARY MATERIALS

The CIF files provided as supplementary materials to the current article include the structure data obtained by refinement of the three samples described above (SoC = 20, 40, and 50%). Combined with well-known structure of LiC_6 these data would be a good starting point for analysis of charged anodes in the whole SoC range between 20 and 100%.

The supplementary material for this article can be found at https://doi.org/10.1017/S0885715617000458.

Bak, S.-M., Hu, E., Zhou, Y., Yu, X., Senanayake, S. D., Cho, S.-J., Kim, K.-B., Chung, K. Y., Yang, X.-Q., and Nam, K.-W. (**2014**). "Structural changes and thermal stability of charged $LiNi_xMn_yCo_zO_2$ cathode materials studied by combined in situ time-resolved XRD and mass spectroscopy," ACS Appl. Mater. Interfaces **6**, 22594–22601.

Billaud, D. and Henry, F. (**2002**). "Structural studies of the stage III lithium–graphite intercalation compound," Solid State Commun. **124**, 299–304.

Billaud, D., Henry, F. X., Lelaurain, M., and Willmann, P. (**1996**). "Revisited structures of dense and dilute stage II lithium-graphite intercalation compounds," J. Phys. Chem. Solids **57**, 775–781.

Bobrikov, I. A., Balagurov, A. M., Hu, C.-W., Lee, C.-H., Chen, T.-Y., Deleg, S., and Balagurov, D. A. (**2014**). "Structural evolution in $LiFePO_4$-based battery materials: *in situ* and *ex situ* time-of-flight neutron diffraction study," J. Power Sources **258**, 356–364.

Casas-Cabanas, M., Reynaud, M., Rikarte, J., Horbach, P., and Rodríguez-Carvajal, J. (**2016**). "FAULTS: a program for refinement of structures with extended defects," J. Appl. Crystallogr. **49**, 2259–2269.

Dittrich, H. and Wohlfahrt-Mehrens, M. (**2001**). "Stacking fault analysis in layered materials," Int. J. Inorg. Mater. **3**, 1137–1142.

Guerard, D. and Herold, A. (**1975**). "Intercalation of lithium into graphite and other carbons", Carbon **13**, 337–345.

He, H., Liu, B., Abouimrane, A., Ren, Y., Liu, Y., Liu, Q., and Chao, Z.-S. (**2015**). "Dynamic lithium intercalation/deintercalation in 18 650 lithium ion battery by time-resolved high energy synchrotron X-ray diffraction," J. Electrochem. Soc. **162**, A2195–A2200.

Iwashita, N., Park, C. R., Fujimoto, H., Shiraishi, M., and Inagaki, M. (**2004**). "Specification for a standard procedure of X-ray diffraction measurements on carbon materials," Carbon **42**, 701–714.

Johnsen, R. E. and Norby, P. (**2013**). "Capillary-based micro-battery cell for *in situ* X-ray powder diffraction studies of working batteries: a study of the initial intercalation and deintercalation of lithium into graphite," J. Appl. Crystallogr. **46**, 1537–1543.

Kleiner, K., Dixon, D., Jakes, P., Melke, J., Yavuz, M., Roth, C., Nikolowskia, K., Liebaub, V., and Ehrenberg, H. (**2015**). "Fatigue of $LiNi_{0.8}Co_{0.15}Al_{0.05}O_2$ in commercial Li ion batteries," J. Power Sources **273**, 70–82.

Kraus, W. and Nolze, G. (**1996**). "*POWDER CELL* – a program for the representation and manipulation of crystal structures and calculation of the resulting X-ray powder patterns," J. Appl. Crystallogr. **29**, 301–303.

Larson, A. C. and Von Dreele, R. B. (**2004**). *General Structure Analysis System* (*GSAS*) (Report LAUR 86-748) (Los Alamos National Laboratory, Los Alamos, New Mexico).

Leoni, M., Gualtieri, A. F., and Roveri, N. (**2004**). "Simultaneous refinement of structure and microstructure of layered materials," J. Appl. Crystallogr. **37**, 166–173.

Li, H., Yang, C., and Liu, F. (**2009**). "Novel method for determining stacking disorder degree in hexagonal graphite by X-ray diffraction," Sci. China Ser. B: Chem. **52**, 174–180.

https://doi.org/10.1017/S0885715617000458 Published online by Cambridge University Press

Ohzuku, T., Iwakoshi, Y., and Sawai, K. (**1993**). "Formation of lithium–graphite intercalation compounds in nonaqueous electrolytes and their application as a negative electrode for a lithium ion (Shuttlecock) cell," J. Electrochem. Soc. **140**, 2490–2498.

Robert, R., Bünzli, C., Berg, E. J., and Novák, P. (**2015**). "Activation mechanism of $LiNi_{0.80}Co_{0.15}Al_{0.05}O_2$: surface and bulk *operando* electrochemical, differential electrochemical mass spectrometry, and X-ray diffraction analyses," Chem. Mater. **27**, 526–536.

Senyshyn, A., Dolotko, O., Mühlbauer, M. J., Nikolowski, K., Fuess, H., and Ehrenberg, H. (**2013**). "Lithium intercalation into graphitic carbons revisited: experimental evidence for twisted bilayer behavior," J. Electrochem. Soc. **160**, A3198–A3205.

Senyshyn, A., Mühlbauer, M. J., Dolotko, O., and Ehrenberg, H. (**2015**). "Low-temperature performance of Li-ion batteries: the behavior of lithiated graphite," J. Power Sources **282**, 235–240.

Sharma, N. and Peterson, V. K. (**2013**). "Overcharging a lithium-ion battery: effect on the Li_xC_6 negative electrode determined by *in situ* neutron diffraction," J. Power Sources **244**, 695–701.

Shi, H., Reimers, J. N., and Dahn, J. R. (**1993**). "Structure-refinement program for disordered carbons," J. Appl. Crystallogr. **26**, 827–836.

Toby, B. H. (**2001**). "*EXPGUI*, a graphical user interface for *GSAS*," J. Appl. Crystallogr. **34**, 210–213.

Treacy, M. M. J., Newsam, J. M., and Deem, M. W. (**1991**). "A general recursion method for calculating diffracted intensities from crystals containing planar faults," Proc. R. Soc. Lond. A **433**, 499–520.

Wilhelm, H. A., Croset, B., and Medjahdi, G. (**2007**). "Proportion and dispersion of rhombohedral sequences in the hexagonal structure of graphite powders," Carbon **45**, 2356–2364.

Zhou, Z., Bouwman, W. G., Schut, H., and Pappas, C. (**2014**). "Interpretation of X-ray diffraction patterns of (nuclear) graphite," Carbon **69**, 17–24.

https://doi.org/10.1017/S0885715617000458 Published online by Cambridge University Press